# Chapter 7
# Map Projections in Planetary Cartography

**Henrik Hargitai, Jue Wang, Philip J. Stooke, Irina Karachevtseva, Akos Kereszturi and Mátyás Gede**

## 7.1 Introduction

### *7.1.1 Historical Background*

The first maps of the Moon showed the Moon in Orthographic projection, as seen by the eye, north up. Riccioli (in 1651) segmented his lunar map into 8 "octants" (Whitaker 2003: 63). Hevelius (1647) used a 360 degree system of azimuths around the limb of the Moon, with the pole of its coordinate system at the sub-Earth point. Tobias Mayer introduced the terrestrial latitude/longitude coordinate system with

H. Hargitai (✉)
NASA Ames Research Center, MS 239-20, Moffett Field,
CA 94035, USA
e-mail: hhargitai@gmail.com

J. Wang
Department of Earth & Planetary Sciences, Washington University
in St. Louis, 1 Brookings Dr., St. Louis, MO 63130, USA

P.J. Stooke
Department of Geography, The University of Western Ontario,
London, ON, Canada

I. Karachevtseva
MIIGAiK Extraterrestrial Laboratory (MExLab), Moscow State University of Geodesy
and Cartography (MIIGAiK), Moscow, Russian Federation

A. Kereszturi
Research Center for Astronomy and Earth Sciences, Konkoly
Thege Miklós Astronomical Institute, Budapest, Hungary

M. Gede
Department of Cartography and Geoinformatics, Eötvös Loránd University,
Budapest, Hungary



M. Lapaine and E.L. Usery (eds.), *Choosing a Map Projection*,
Lecture Notes in Geoinformation and Cartography,
DOI 10.1007/978-3-319-51835-0_7

meridians and equator (Greeley and Batson 1990: 147). The orientation was changed to south up by Schröter, showing the view as seen through an astronomic telescope (Mayer and Schröter 1791). This system remained in use until 1961. Lunar directions were stated with reference to their position in the sky as viewed from the surface of the Earth. Mare Orientale, the "Eastern Sea," is on the left limb of the Moon as seen in the Northern Hemisphere, that is, toward the east horizon. The orientation of Lunar maps was changed in 1961, when the "astronautical convention" was adopted in anticipation of human spaceflight. The direction from which the Sun rises on the Moon was henceforth called east, as it is on the Earth. This also reflected the fact that with the coming of Space Age, observations of the Moon were not relied on astronomic telescopes, but on spacecraft imagery instead. Map orientation was changed back to north up as in the very early decades of Lunar observations (Wilhelms 1987: 11).

Size and shape information, directions of the poles of rotation and definition of prime meridians of the planets and satellites have been published by the International Astronomical Union (IAU) Working Group on Cartographic Coordinates and Rotational Elements (WGCCRE) since 1979, with the addition of the same data for small bodies: minor planets (asteroids) and their satellites, and comets since 2003 and dwarf planets since 2009. This database is revised every three years (Archinal et al. 2011). The working group recommends a specific cartographic coordinate system for each body, although alternative coordinate systems may exist for various (e.g. dynamical) purposes. The mission of the working group is "to make recommendations that define and relate the coordinate systems of Solar System bodies to their rotational elements to support making cartographic products" of such bodies in a standardized way. High precision coordinates are essential for spacecraft operations, high-resolution mapping, and gravity field determination (Archinal et al. 2011).

### *7.1.2 Basic Terminology*

Before the space age, unique prefixes like seleno- (Lunar) or areo- (Martian) were in use for each planetary body (e.g., Selenography, Areography) and these disciplines mainly dealt with the description of surface features, similar to what geography did at that time for Earth. Today most commonly the prefix geo- is used for any solid body considered under the umbrella term *planetary science*. This reflects the comparative planetological approach according to which the principles of terrestrial geology can be transferred to any other planets (Wilhelms 1990: 209). Unique prefixes or suffixes, however, are still used in some terms referring to coordinates, control points and global figures (with endings like -graphic, -centric, -detic, -id etc.). Coordinate systems are usually referred to as planetographic or planetocentric coordinates; however, in some cases the following prefixes are used: areo- (Martian), seleno- (Lunar), helio- (Solar), zeno- (Jovian) and geo-(Terrestrial).

In the following sections we present an overview of various cartographic aspects of the maps of solid-surface planets, gas giants, satellites, and small bodies with special emphasis on the projections of the end products. Finally, we discuss map-projected planetary images.

## 7.2 Planets

### *7.2.1 Rotation*

The rotation of a planet may be direct (or prograde, or eastward or positive) or retrograde, depending on the direction of rotation (the Earth and the Sun rotate directly) (Archinal et al. 2011). Direct rotation is counterclockwise when viewed from above the north pole (JPL 2009).

### *7.2.2 Coordinate Systems*

Planetary coordinate systems are defined relative to their rotational axis (that defines the latitudes) and prime meridian (Archinal et al. 2011). In planetary cartography two coordinate systems are used that are fixed to the body: the planetographic coordinate system (IAU 1971) and the planetocentric coordinate system. In both cases, the origin is the center of mass of the body. The coordinates of a planetocentric or spherical coordinate system are defined by a vector from the center of mass of the body to a particular point, while the planetographic coordinates are defined by a vector perpendicular to a reference surface (JPL 2009) (Fig. 7.1). The planetographic and planetocentric vectors are identical if the reference surface is a sphere (JPL 2009; Roatsch et al. 2008). On an oblate spheroid typical of rapidly rotating planetary objects such as Earth and Mars, both vectors are identical at the poles and equator, but the planetographic latitude at a given point in intermediate latitudes is larger than the planetocentric value. On Mars, for example, the difference between the latitudes amounts to approximately 0.3° (20 km) at 45° and vanishes at the equator and poles (Rosiek et al. 2005). A list of currently IAU-accepted coordinate systems for the planets and satellites is found at http://planetarynames.wr.usgs.gov/TargetCoordinates.

In terrestrial geodesy and in a spherical or planetocentric coordinate system, longitudes are always positive toward the east as defined by the “right-hand rule” (Archinal et al. 2011). An external observer would see planetocentric longitudes to decrease with time for directly rotating bodies (JPL 2009). This system is independent of the definition of the reference ellipsoid (Duxbury et al. 2002).

In a planetographic system, the range of longitudes extends from 0° to 360°. The planetographic longitude of the central (e.g., sub-Earth) meridian, as observed from

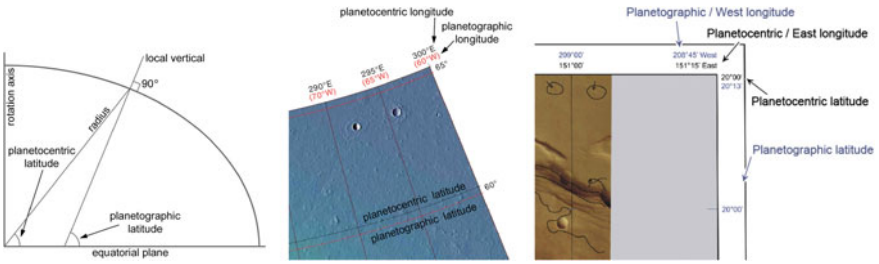


**Fig. 7.1** Planetocentric and planetographic coordinates. *Left:* Geometric distinction between planetocentric and planetographic latitudes. The degree of polar flattening of this cross-section is greatly exaggerated. *Center:* Detail from the 1:5 M MOLA-based topographic map of the MC3 Arcadia Quadrangle of Mars that was made to show the official nomenclature and displays both sets of coordinates (USGS n.d.). This map has been replaced by a THEMIS-based map in 2014 that only displays planetocentric East coordinates. *Right:* Dual coordinates shown on the ortophoto-mosaic map of Albor Tholus, compiled at the Technical University of Berlin (Alberz et al. 2004a, b)

a direction fixed with respect to an inertial system, will increase with time (Archinal et al. 2011). This is the case in observing a planet's rotation from the Earth that explains why this system was chosen traditionally for mapping planetary bodies through telescopes from Earth.

Thus, west longitudes that are measured positively to the west are used for bodies with direct rotation, and east longitudes measured positively to the east when the rotation is retrograde, except for the Earth, Moon, Sun which have longitudes run both east and west 180°, or east 360° for historical reasons (Archinal et al. 2011).

Traditionally the planetographic system with west-positive ("west-'ographic") coordinates has been used for the mapping of planetary bodies. An areographic system was used for maps of Mars produced from the 1970s through the late 1990s (Duxbury et al. 2002). However, several recent missions adopted the planetocentric, east-positive ("east-'ocentric") system (Archinal et al. 2011). An areocentric system with east-positive longitudes was introduced with the Mars Global Surveyor (MGS) mission's MOLA (Mars Orbiter Laser Altimeter) team whose product, the MOLA grid, serves as a standard of geodetic control (Duxbury et al. 2002). This system was adapted in subsequent missions, including the US Mars Odyssey, European Space Agency's Mars Express (Gehrke et al. 2003), and US Mars Reconnaissance Orbiter missions. The MESSENGER mission adopted the planetocentric system for Mercury (Seidelmann et al. 2007). The Lunar Reconnaissance Orbiter mission recommended the planetocentric coordinates and east-positive longitude from 0° to 360° range for Lunar mapping, breaking the Lunar traditions (LGCWG 2008).

The IAU Working Group on Cartographic Coordinates and Rotational Elements allows the use of either planetographic or planetocentric system for a given body (JPL 2009). For Mars, both traditionally used planetographic latitudes with

west-positive longitude (Inge and Batson 1992) (control network: MDIM (Mosaiced Digital Image Model) 1.0 or MDIM 2.0), and planetocentric latitudes with east-positive longitude (MDIM 2.1) co-existed in the 2000s, although the planetographic system has been dropped in most newer maps. The Mars Transverse Mercator (MTM) Map Series in which geologic and controlled photomosaic maps are published since 1984, have been updated using the planetocentric coordinates as the primary grid with a secondary grid showing the planetographic coordinates (Rosiek et al. 2003) (Fig. 7.1, Center), and HRSC maps use a similar dual system (Fig. 7.1, Right).

Most commercially available GIS systems (without special plug-ins) don't support the 0–360° longitude range and the west-positive longitude system. Mapping with the −180 to +180° east-positive coordinate system is recommended even if the final product will be labelled differently.

#### 7.2.2.1 Prime Meridian/Fixed Reference Feature

A dynamically defined coordinate system does not suit the needs of mapping of surface features, therefore body-fixed, mass-centered coordinate systems are recommended for rocky bodies. The prime meridian of most rocky planets is defined arbitrary, usually by references to a suitable, prominent or easily observable surface feature such as a circular crater whose center point can be easily determined. This fixed reference feature may or may not be located on the prime meridian. As long as the original definition is maintained to within the accuracy of previous determinations, smaller features may be chosen to define the origin for longitude more precisely (Archinal et al. 2011).

The prime meridian of Mars was first defined by the German astronomers Beer and Mädler in 1830–32, who used a small dark feature to determine the rotational period of Mars. Later observers adapted this reference point that was named Dawes' Forked Bay by Proctor in 1864 (Proctor 1873) and Baie du Méridien by Flammarion (1890) after the bay-like appearance of the feature on Dawes' 1864 Mars drawings (Flammarion 1888 [1978]). The name was later latinized to Sinus Meridiani, by Antoniadi (1930) ('Meridian Bay', similar to Sinus Medii ['Middle Bay'] on the Moon).

After the Mariner-9 mission, it was redefined and fixed to the center of the small crater Airy-0 (de Vaucouleurs et al. 1973) by Merton Davies (MSSS 2001), a small crater inside the larger Airy crater, whose name commemorates GB Airy, who established Greenwich as the location of the prime meridian on Earth. Both craters are shown in Fig. 7.2.

For Mercury, the center of Hun Kal crater was used to define the 20°W longitude and it served as a reference to locate the prime meridian. Hun Kal means the 'number 20' in Mayan. This crater is shown in Fig. 7.3.

The rotation period of Venus was first determined from radar data in 1964, and the zero meridian was set to run through one of the first radar-bright features to be located (Carpenter 1966), later called Alpha (today's Alpha Regio). This feature

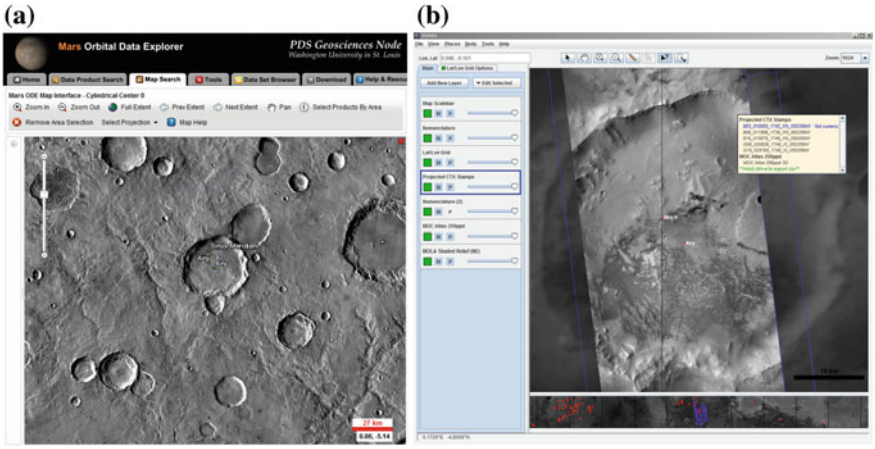


**Fig. 7.2** Airy-0 and Airy craterson Mars. Screen copies from two GIS systems: **a** the NASA's Planetary Data System (PDS) Orbital Data Explorer (ODE). The basemap is Mars Odyssey THEMIS (Thermal Emission Imaging System) day IR (infrared) global mosaic generated by the Arizona State University THEMIS team (NASA's PDS Geosciences Node). **b** JMARS (Christensen et al. 2009) showing closeup of Airy crater in CTX image B03_010855_1742_XN_05S359W on MOC photomosaic background (NASA, JPL, Malin Space Science System)

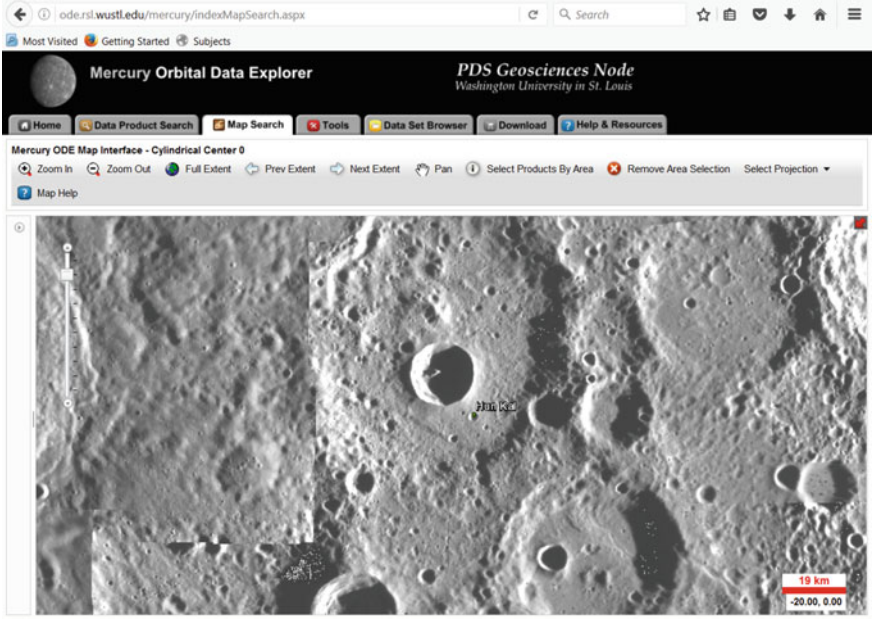


**Fig. 7.3** Hun Kal crater on Mercury. The basemap was created using MESSENGER (Mercury Surface, Space Environment, Geochemistry and Ranging) orbital images including MDIS (Mercury Dual Imaging System) Narrow Angle Camera (NAC) and Wide Angle Camera (WAC) images. The map was generated by NASA's MESSENGER mission team and cartographic experts from the U. S. Geological Survey (USGS) (NASA's PDS Geosciences Node)

faced Earth at the inferior conjunction in 1964 and approximately in later years, since the rotation is nearly but not exactly resonant (IAU 1971: 128).

Because of uncertainties of the rotational period, a new definition based on a prominent surface feature was created in 1985. D. Campbell and Y. Tjuflin selected six craters that are common to both Russian Venera and American Arecibo datasets and selected one, named Eve (Davies and Rogers 1991). It was later replaced by another crater on the same longitude, so it passes the central peak of Ariadne crater at latitude 43.8°N (Hirsch 1994) (Fig. 7.4).

Unlike most other planets, Venus has a naturally defined particular meridian that has a special importance: this meridian corresponds to the sub-Earth longitude at the inferior conjunction (cf. Marov et al. 1973). When every 583 days Venus is positioned between the Earth and the Sun, the hemisphere of Venus centered at 320°E longitude turns toward the Earth (Burba 1996). This peculiarity can be visualized when selecting the cartographic central meridian of Venus or its hemispheres: 320° and 140°E longitudes are in fact used as the central meridians for the Venus relief map compiled in Lambert Azimuthal Equal Area projection (Lazarev and Rodionova 2011).

Pluto forms a double planet with its largest moon, Charon. They are tidally locked in a synchronous orbit, in other words, they face each other continuously. No other planet (or known dwarf planet) in the Solar System is tidally locked to its moon. The prime meridian of Pluto is crossing the sub-Charon point. The definition of Pluto's coordinate system is especially complicated (Zangari 2015).

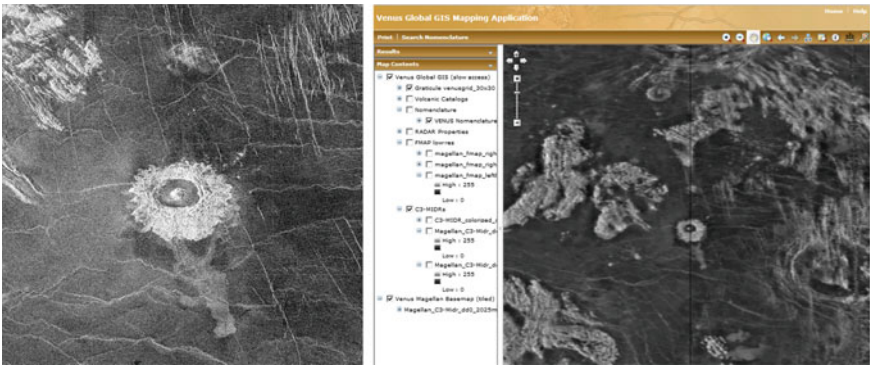


**Fig. 7.4** *Left* Ariadne crater in Venus Magellan Synthetic aperture radar (SAR) FMAP left-look (full-resolution left-looking map) image mosaic created by the USGS Astrogeology Research Program (from Map-a-Planet of NASA's PDS Imaging Node). *Right* A broader geological context is shown in the display of the Venus Global GIS Mapping Application of UGSG in Equidistant Cylindrical projection

#### 7.2.2.2 Latitude Systems

The North Pole is the pole of rotation that lies on the north side of the invariable plane of the Solar System which is close to but not the same as the ecliptic (JPL 2009). The direction of the North Pole at a given epoch is specified by the value of its right ascension $\alpha_0$ and declination $\delta_0$ (Archinal et al. 2011). North latitudes are designated as positive.

### *7.2.3 Topographic Reference Surfaces*

Traditionally a spherical or ellipsoidal shape is used for mapping. Earth (geoid) and Mars (areoid) have datums that are rotational ellipsoids for which the radius at the equator is larger than the polar semi-axis (Archinal et al. 2011). The Mars reference body was redefined several times by the improved data on the planet's shape (Davies et al. 1992, 1995). The current version is defined by IAU as the "Mars IAU 2000" ellipsoid (Seidelmann et al. 2002). On Mars, the zero elevation level is defined by the mean planetary radius. The zero elevation of previous models of the Mars topography (Wu 1991), coincides with the average atmospheric pressure (6.1 mbar) measured by Mariner 9 probe (Zuber and Smith 1998; Kliore et al. 1972). MOLA topography is believed to be a significant improvement over previous models and was related to the 6.1 mbar atmospheric pressure surface of Mars by Zuber and Smith (1998).

Standard models of the reference surface are digital terrain models (DTMs). A DTM defines body radius or geometric height above the body reference surface as a function of cartographic latitude and longitude (JPL 2009). Laser altimetry based accurate topographic data is available for Mars (MOLA), Mercury (MLA) (Neumann et al. 2011) and Moon (LOLA: Lunar Orbiter Laser Altimeter) (Smith et al. 2010), while radar altimeters surveyed the topography of Venus (Muhleman 1961; Campbell et al. 1976).

Horizontal and vertical control bases for Mars topographic mapping are provided by the 231 m/pixel MDIMs generated from Mariner 9 and Viking Orbiter imagery and 500 m/pixel MGS MOLA grid (Archinal et al. 2004; Rosiek et al. 2005). The MOLA ground point spacing is about 300 m along track and 1/64 degree across track. This causes a wide spacing in the equatorial zone, which results in interpolation artifacts in the data gaps (Gwinner et al. 2010). The MOLA radii have accuracy $\sim$10 m vertically and $\sim$100 m horizontally (Neumann et al. 2001). A Martian areoid is generated from the original MOLA points and can be downloaded from the PDS Geosciences Node at a resolution of 32, 64 and 128 pixel/degree. MOLA data are considered the best Mars global control up to date. The MOLA global topographic map was generated by the MOLA science team as shown in Fig. 7.5.

In addition to the MOLA-based DTMs, other high resolution DTMs produced from the Mars Express High-Resolution Stereo Camera (HRSC) stereo images and

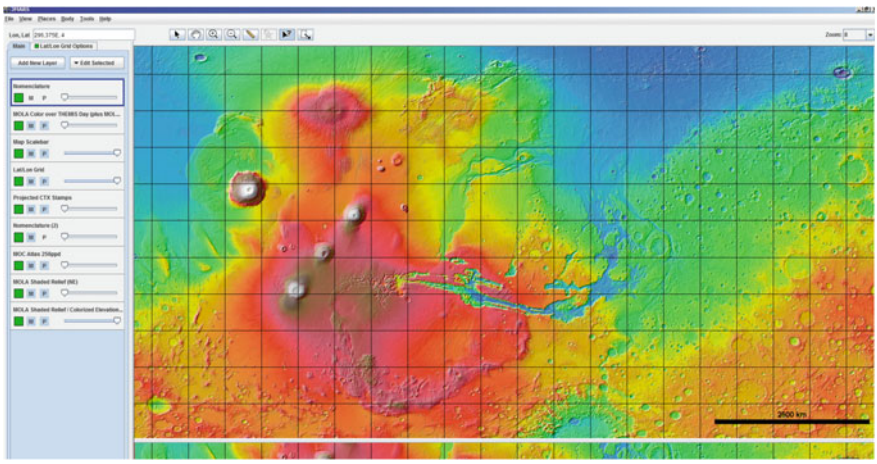

**Fig. 7.5** Mars global surveyor MOLA global topographic map displayed in JMARS (MOLA Science Team) (Smith et al. 1999; Christensen et al. 2009)

the Mars Reconnaissance Orbiter HiRISE stereos (McEwen et al. 2007) are widely used. The HiRISE stereo pair is triangulated and controlled to MOLA elevation values, when possible (Eliason et al. 2006). HiRISE DTMs have a spatial resolution around 1–2 m. HRSC DTMs have a spatial resolution around 200 m, depending on the version and algorithm of the produced dataset. The HRSC DTM has a more accurate representation of areas with strong relief, whereas the MOLA DTM is often more reliable on level and very smooth terrain as well as on ice surfaces, because stereo image correlation may fail completely without visible albedo or morphologic features (Gwinner et al. 2010).

### *7.2.4 Projections*

*For small scale* (*global*) *maps* Batson (1990) recommends the Lambert Azimuthal Equal-Area projection that retains the area of features, regardless of location, but it distorts the shapes and craters appear as ellipses at the edge of the map. This phenomenon of apparent foreshortening is well known in orthographic projections or by direct observations of the Moon. This effect gives the user a spherical feeling of the map. This projection is used in two-hemisphere views of the three series of the "Multilingual Maps of the Terrestrial Planets and Their Moons" (Dresden series: Shingareva et al. (2005), Budapest series: Hargitai and Bérczi (2006); Children's map series: Hargitai et al. (2015), Fig. 7.6—all three series are supported by ICA Commission on Planetary Cartography).

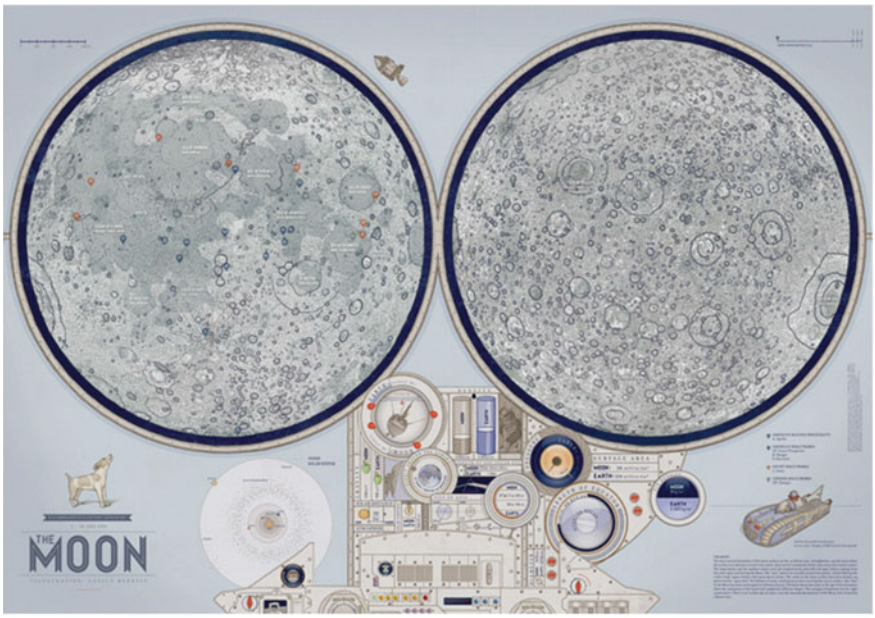


**Fig. 7.6** Map of the Moon, designed by L. Herbszt (Hargitai et al. 2015). Lambert Azimuthal Equal-Area projection

Global small-scale maps, especially thematic maps, typically use the Mercator (e.g., Wilson 1912) or Equirectangular projection. Polar views may be shown in Azimuthal Equidistant or Polar Stereographic projection (Fig. 7.7).

The *Orthographic projection* provides a visually attractive global view, but the entire surface of a body can only be displayed in three views, and limb portions are heavily distorted. For global figures, the *Robinson projection* is increasingly popular. A recent example is the new global Geologic map of Mars (Tanaka et al. 2014).

*For systematic mapping*, the planet may be divided into projection zones: the Mercator projection is used in equatorial latitudes (e.g., 0–30°); the Lambert Conformal Conic in mid-latitudes (e.g., 30–65°) and the Polar Stereographic in polar latitudes (Batson 1990) (e.g., 65–90°) (examples of latitudinal ranges are from MOLA 1:5 M atlas).

*Digital, interactive applications* typically display maps in a simple cylindrical (equirectangular) "database-" or on-the-fly projections, or the sinusoidal projection (an equal-area projection, used for tiled data products), equally sampled in either planetographic or planetocentric latitudes. In these interactive digital GIS applications the users may modify or re-center the projection according to their needs.

The NASA's PDS Imaging Node has developed an online tool called "Map-a-Planet" to extract science-ready, map-projected images from global mosaics (Akins et al. 2014). This tool can display user-defined portions of 16-planetary

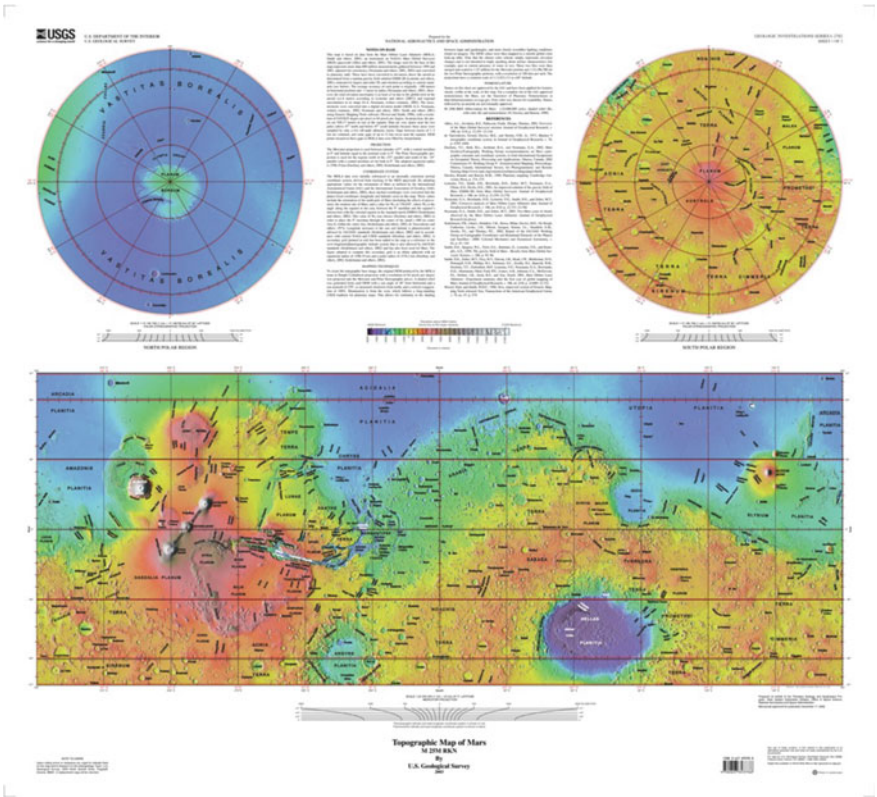


**Fig. 7.7** MGS MOLA topographic map in print. Mercator projection 0 ± 57°, polar stereographic ±57–90° (USGS 2003). Cf. the digital version in Figs. 7.5 and 7.9

bodies in several thematic layers or image bands. Map outputs can be selected from four projections. In the Sinusoidal Equal-area projection Map-a-Planet always uses a central meridian at the center of the image map, in order to minimize map distortion. In the Simple Cylindrical projection features on a planet, such as round impact craters, become flattened at the higher latitudes. In the Mercator projection polar regions are extremely distorted but angles and shapes within any small area are essentially true. The Polar stereographic projection can be pre-ordered for a later download. Examples of different projections of a cratered surface, the Schrödinger Basin (75.0°S 132.4°E) region on the Moon are show in Fig. 7.8 (planets have similar viewing options). Map-a-planet 2 (https://astrogeology.usgs.gov/tools/map-a-planet-2) has been in operation since 2015 in order to replace the old version of Map-a-planet (Akins et al. 2014).

JMARS is a cross-platform GIS application developed by the Mars Space Flight Facility (Christensen et al. 2009). When started, data is displayed in Equirectangular Projection centered and projected at 0°E, 0°N. Users can re-project the maps with the center of the viewing window as the new center-point (Fig. 7.9).

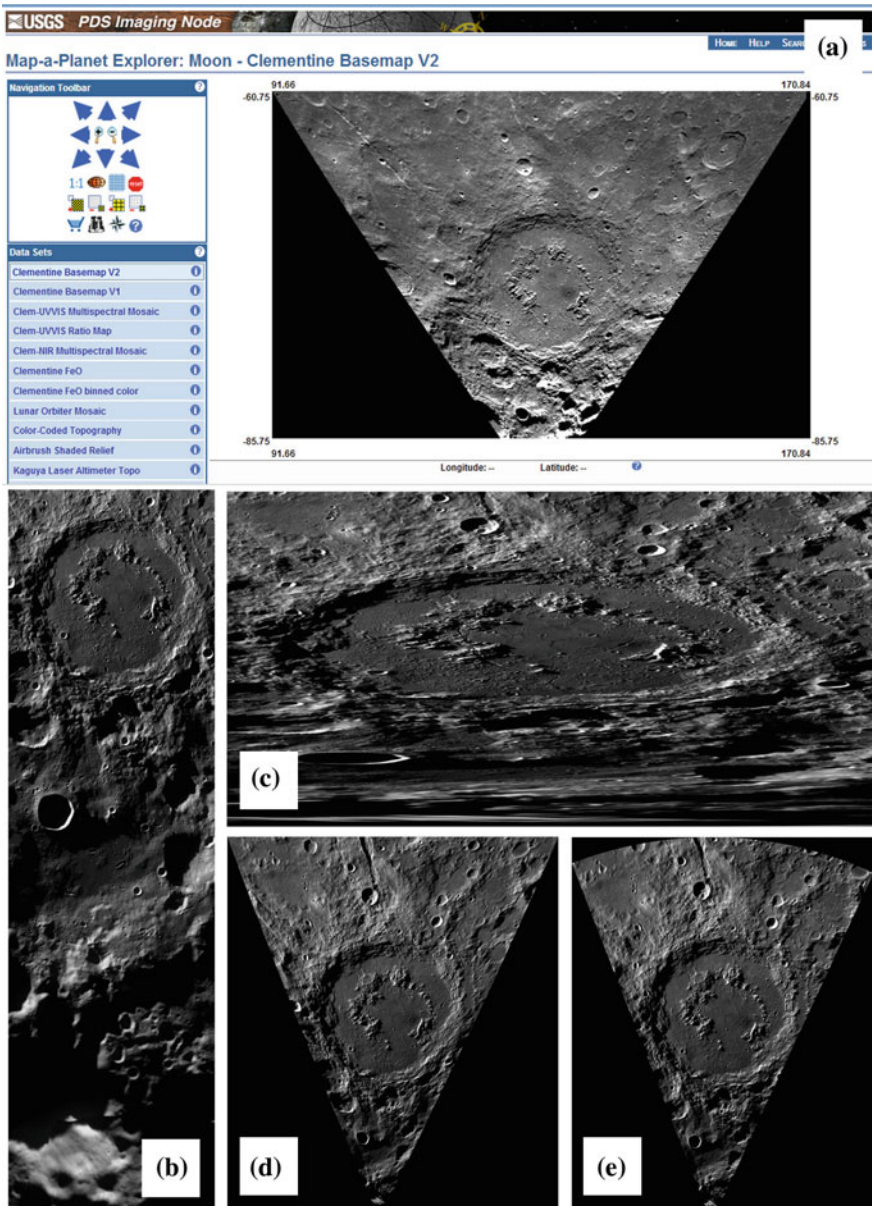


**Fig. 7.8** **a** Map-a-planet: Schrödinger Basin in Clementine Basemap in sinusoidal equal-area projection (NASA's PDS Imaging Node, captured in 2013.). **b–d** The same crater in Lunar Reconnaissance Orbiter Camera Wide Angle Camera mosaic, produced in Map a Planet 2, 2017. **b** Mercator Projection, **c** Simple Cylindrical Projection, **d** Sinusoidal Equal-Area Projection, **e** Polar Stereographic Projection

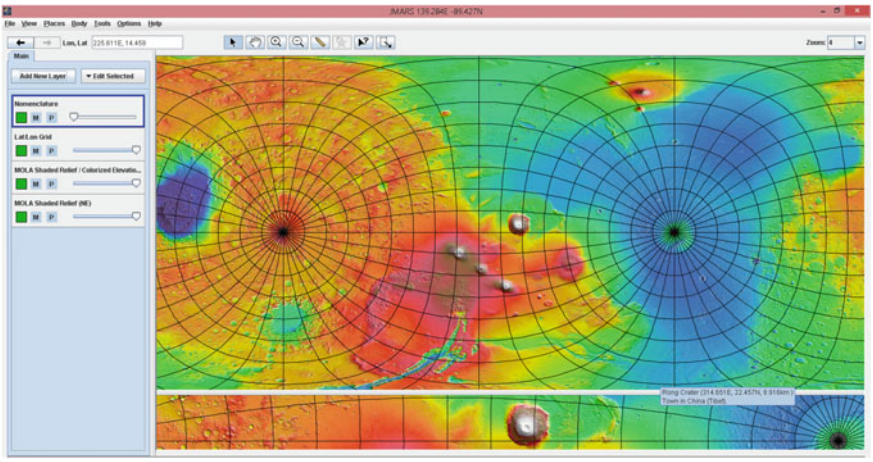

**Fig. 7.9** Reprojected image of that in Fig. 7.5 in JMARS, re-centered at the southern pole

Finally, Esri's ArcGIS Online platform offers planetary maps and map layers (global background maps, quad chart gridlines etc.) from several Web Map Servers maintained by universities or research institutions. These can be directly imported into ArcMap in any projection.

*Printed (or static, pdf) maps*, however, traditionally use *conformal projections* (Mercator, Transversal Mercator, Lambert Conformal Conic, Polar Stereographic) which have no distortion of the shape and are independent of the actual—planetocentric or planetographic—coordinate system (Duxbury et al. 2002). Conformal projections are favored by astrogeologists because shape information is essential in interpreting surface features by photogeologic methods (Batson 1990). One particularly important landform in this respect is impact craters that are circular in shape. As it is put by Veverka (1985) when speaking of the choose of conformal projections: "most of us like to see round craters round". Distortion-free shape is especially important for precise measurements, like those made in the statistical analysis of crater size-frequency distributions where incorrect diameter measurements due to map distortions may lead to younger or older extracted surface ages. Distortions of diameters and areas within different map projections cause considerable errors during such measurements. In order to address this problem, an ArcGIS software module, called CraterTools, was developed by Kneissl et al. (2011) in which impact crater images are internally projected to a stereographic map projection with the crater's central-point set as the projection center, where the circle is defined without any distortion of its shape. The diameter is then measured using a sinusoidal map projection with a center longitude set to the crater's central-point, which does not show any distortion. *Equal-area projections* are useful in evaluating distribution, density and area of surface features (Batson 1990). The 1:200000 topographic image map series based on Mars Express HRSC imagery used equal-area map projections: sinusoidal projection between 85°N and 85°S,

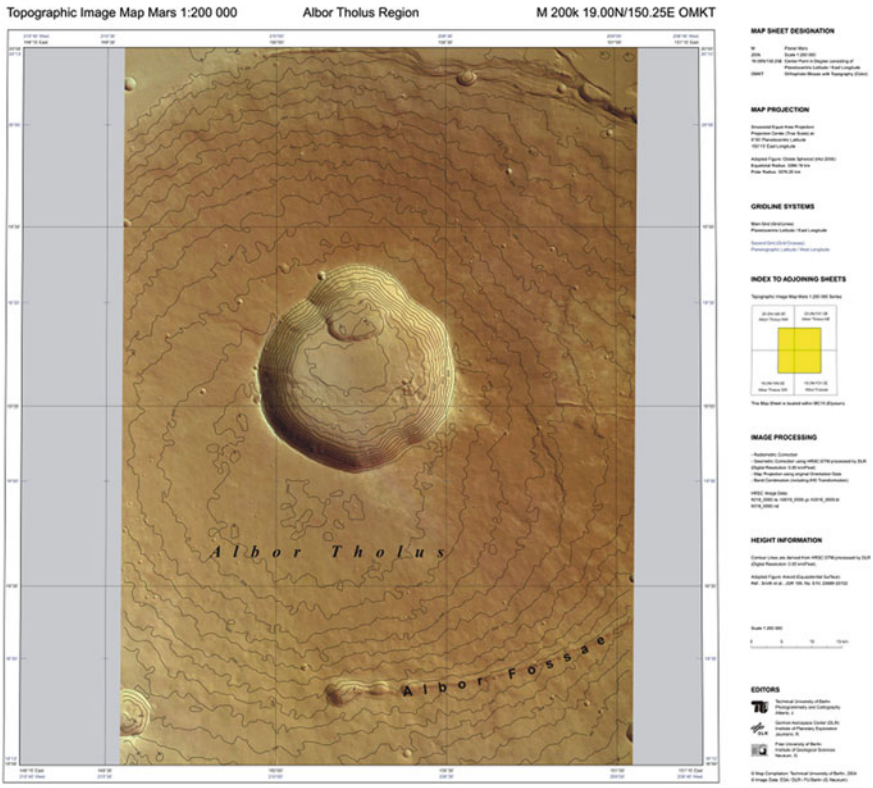


**Fig. 7.10** HRSC 1:200000 topographic image map M 200k 19.0N/150.3E OMKT of Albor Tholus, Mars (Alberz et al. 2004a, Sinusoidal equal area projection

and Lambert Azimuthal projection for the polar areas (Alberz et al. 2004a, b) (Fig. 7.10).

*Globes*: traditional globe map prints usually consist of 12 gores (sometimes 9 on very small globes or 18 on very large globes) completed with two polar caps. The gores are in Cassini projection (transverse form of Simple Cylindrical projection) or in another similar projection such as Polyconic with central longitudes matching the central longitudes of the gores, while the projection of polar caps (usually stretching to the 80° or 70° latitude) is Azimuthal Equidistant (Wagner 1962). A globe map example is shown in Fig. 7.11.

*Virtual globes*: Google Earth's digitized globe uses Simple Cylindrical (Plate Carrée) projection for its imagery base including all add-on planetary maps. These maps are further reprojected into a General Perspective projection for viewing (Di Palma 2009). The General Perspective projection is similar to the orthographic projection, but its point of perspective is located at a scalable and finite distance. In Google 2D Maps (Earth, Mars and the Moon), the Mercator projection is used from the equator to approximately ±85° ($y$ coordinates of the poles are infinite in the Mercator projection so the mapping limits are set to have the whole map

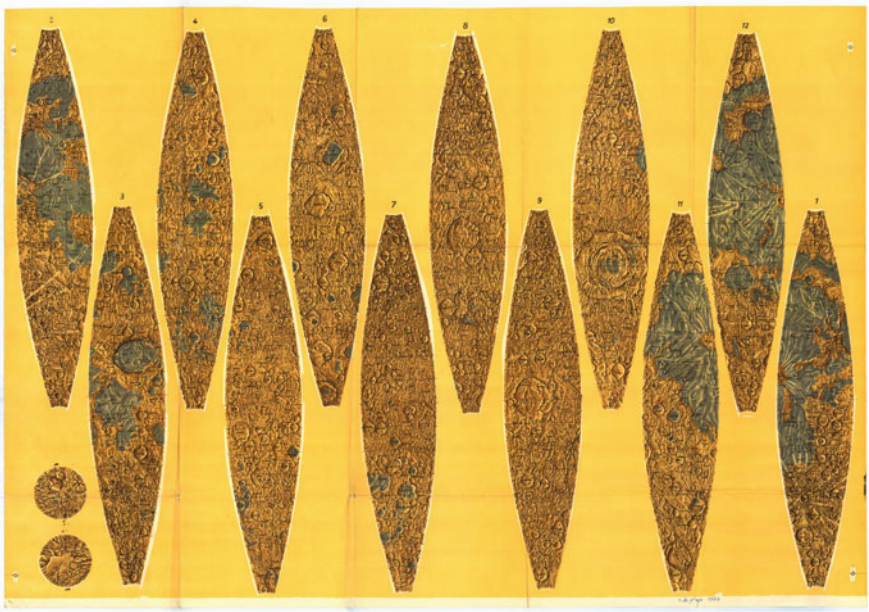

**Fig. 7.11** Räths Erdmondglobus. VEB Räthgloben-Verlag, Leipzig, 1976; Courtesy of the Department of Cartography and Geoinformatics, Eötvös Loránd University

square-shaped). Due to technical reasons, longitudes may run over ±180° when defining features across the 180° longitude. Although the projection can be customized in Google Maps, using a custom projections requires new raster tile sets as the built-in map types are provided only in the Mercator projection. Another limitation is that custom projections are assumed to be rectilinear (i.e. x is a function of the longitude and y is a function of the latitude only). Defining non-rectilinear (e.g. azimuthal) projection is possible but the map interface will behave incorrectly (Google 2012).

VRML/X3D globes of the Virtual Globes Museum (VGM) (Márton 2008) use maps in three different projections to improve visualization and optimize texture sizes: two azimuthal equidistant maps for the polar regions and a Plate Carrée map between the ±50° latitudes (Gede 2009).

Regardless of the target virtual globe applications, globe maps have to be compiled keeping the distortions in mind. As for instance, when stretching a Plate Carrée map to the virtual globe, distances along the latitudes are reduced by cos $\varphi$ times—above 60° the reduced width is less than half of the original which makes especially symbols and labels very distorted. In order to prevent these errors Hargitai and Gede (2009) recommended compiling maps of the higher latitudes in azimuthal equidistant projection and a Plate Carrée map for the equatorial regions, similarly to maps used in the VGM. Labels beyond the 30° latitude on the Plate Carée map should be horizontally stretched by cos $\varphi$ and diagonally placed labels should be avoided if possible.

## 7.3 Gas Giant-Specific Parameters

### *7.3.1 Longitude System*

The rotation of those bodies that have no solid surface (gaseous giant planets) can be either defined by the apparent rotation of the equatorial (System I) and mid-latitude (System II) cloud tops (for Jupiter) or by the rotation of their internal magnetic fields (System III) as determined by their radio signals during fly-by or orbital missions (Newburn and Gulkis 1973)

### *7.3.2 Size and Shape*

The radii and axes of the large gaseous planets are determined at the one-bar-pressure surface. (Archinal et al. 2011).

Stellar occultations are often used to analyze the atmospheric structure of giant planets, and these measurements also provide information on the shape of the planetary body (Lecacheux et al. 1973), while analysis of probes orbiting around giant planets as well as the orbital changes of those probes that pass by them are used to analyze their field of gravity, and the inferred oblateness of their shape (Null 1976). Beside these methods, the shape determinations are completed by theoretical calculations using rotational speed of interior (observed by changes in the radio wavelength) (Anderson 1975) and correlating the oblateness with models of internal structure and hydrodynamic behavior of the fluid interiors (Helled et al. 2010).

## 7.4 Satellite-Specific Parameters

### *7.4.1 Longitude System*

The axis of rotation of most satellites is normal to the mean orbital plane of the satellite. The rotation rate of most satellites is equal to their mean orbital period (i.e. they have a synchronous rotation due to tidal locking). Since on the tidally locked satellites there is a specific point located at a particular longitude defined by physical parameters, the positioning of the prime meridian on these bodies is not arbitrary. It is determined by the mean sub-planetary point (i.e. the center point of the hemisphere that always faces the parent body). Nevertheless, in most cases there is typically an impact crater at an arbitrary longitude that defines the longitude system, for example the Cilix crater on Europa that defines the 182° meridian (Archinal et al. 2011). On Io there are no impact craters observed yet and its surface is being actively resurfaced and thus modified by volcanism, so the 0° meridian is

not fixed to a surface feature, but has been defined using the astronomical definition: the prime meridian of Io is the sub-Jupiter longitude at the first superior conjunction after 1950.0 (Veverka 1985).

### 7.4.2 Reference Surfaces

Although calculations predict that the hydrostatic shapes of several mid-sized and large satellites are triaxial ellipsoids, spherical reference surfaces are used due to complicated computation of triaxial ellipsoids and lack of agreement on basic definitions like longitude and latitude (Archinal et al. 2011). A spherical reference surface has the advantage that planetographic and planetocentric latitudes are numerically equal (Roatsch et al. 2008).

The shape determination series of satellite images are also used, especially from such missions where the probes orbited around a giant planet: Galileo around Jupiter (Davies et al. 1997) and Cassini around Saturn (Davies and Katayama 1984). In the cases of small or poorly imaged/visited satellites basic parameters like radius might contain substantial uncertainty.

Laser altimetry based accurate LOLA topographic data are available for the Moon (Smith et al. 2010), while radar altimeters surveyed the topography of Titan locally, by Cassini Radar (Radebaugh et al. 2007).

For most of the Solar System bodies no accurate topographic data are available, and shapes are determined using images of limb shapes (Thomas 1989), terminator positions, with methods of shape from shading (Lohse et al. 2006) and stereo image pair analysis. Numerical shape models are generated using these data (Simonelli et al. 1993).

### 7.4.3 Projections

Kaguya terrain camera images of the Moon are map-projected similarly, in simple cylindrical projection. Global mosaic maps of the Saturnian satellites from the Cassini mission are prepared in simple cylindrical projection. These serve both scientific interpretation and future mission planning (Gehrke et al. 2006).

## 7.5 Small/Irregular Body Specific Parameters

### 7.5.1 Rotation

The North Pole may change into South Pole for some of the comets with very large precession over a few decades (Archinal et al. 2011). In the case of some asteroids, rotation around several (usually two) axes might be present (Harris 1994).

### 7.5.2 Coordinates

In some cases, two coordinates may not be enough to uniquely identify a surface point, because a line from the center of the object may intersect the surface more than once. Examples are Eros, Kleopatra, Itokawa and possibly Toutatis and Ida (Archinal et al. 2011).

#### 7.5.2.1 Longitude

For irregular bodies, the prime meridian may be chosen to align with its longest axis (e.g., 433 Eros). In the case of irregular bodies, it is desirable to relate each of its coordinate axes to a prominent landmark feature, rather than a single feature that defines a prime meridian, because their rotational axes and rates may be poorly defined or may vary in time. Currently, the 0° meridian is defined in a variety of ways for small bodies, including a bright albedo feature (Ceres); the direction of the long axis (Pallas); an arbitrary selected point based on light curve information (Lutetia); an arbitrary selected date on which the direction of the long axis pointed toward the Earth (Davida); the mean sub-body meridian (Pluto, Charon); impact craters (Eros, Ida) and other circular features. It is recommended that small bodies have an east-positive system that run 0–360° (Archinal et al. 2011).

### 7.5.3 Reference Surfaces

For convenience, sometimes spherical reference surfaces are used for mapping purposes (Archinal et al. 2011). In a few cases shapes could be determined by radar observation when the given asteroid has close flyby the Earth (Ostro et al. 1999). In such cases the coverage is poor if the rotation of the body is slow and the resolution is inhomogeneous because its distance from the Earth changed during the observation. The most detailed shape models for small and irregular bodies are available for Phobos (Willner et al. 2010) and Eros (Thomas et al. 2002) that have been imaged from close orbits.

### 7.5.4 Projections

Orthographic projections are convenient (Archinal et al. 2011) but they are redundant because six views are needed for a good surface coverage (Stooke 1992). The earliest maps of irregular bodies were sketches on unmodified cylindrical and azimuthal projections on a sphere (e.g., the map of Phobos in 1974 and Amalthea in 1981), containing large distortions. Modified cylindrical projections were

developed by John Snyder and Lev Bugaevsky (Bugaevsky 1987). Unlike Snyder, Bugaevsky used planetocentric coordinate system that was implemented for Soviet maps of Phobos during planning research experiments of Phobos-1,-2 missions (Bugaevsky et al. 1992) and later it was used in the Atlas of Terrestrial Planets (Marov et al. 1992). The modified Bugaevskiy projection represents a real shape of the irregular celestial body (the parallels are sinusoidal) and is based on analytical method of calculations (Bugaevsky 1999; Fleis 2004). The modified Bugaevskiy projection is also used for the most recent mapping of Phobos (Fig. 7.12), based on Mars Express SRC (Super-Resolution Channel) orthoimages (Karachevtseva et al. 2015) and accessible online (Nyrtsov et al. 2012; http://geocnt.geonet.ru/en/3_axial).

Stooke (1992) developed a so-called morphographic azimuthal projection in which the radius constant of the spherical projection is replaced with a local radius. The coordinate grid is modified to follow topographic features, being pushed out from the centre of the map by larger radii and pulled towards the centre by smaller radii, enhancing global shape visualization and allowing the outer boundary of a map of a hemisphere to duplicate the shape of the cross-section of an object. Traditional cylindrical and conic projections designed for use with spherical objects were also adapted to irregular objects by Nyrtsov and Stooke (2002). An equal-area mapping technique is described by Berthoud (2005). The equal area projection retains the true relationship of areas and is useful in estimating the surface

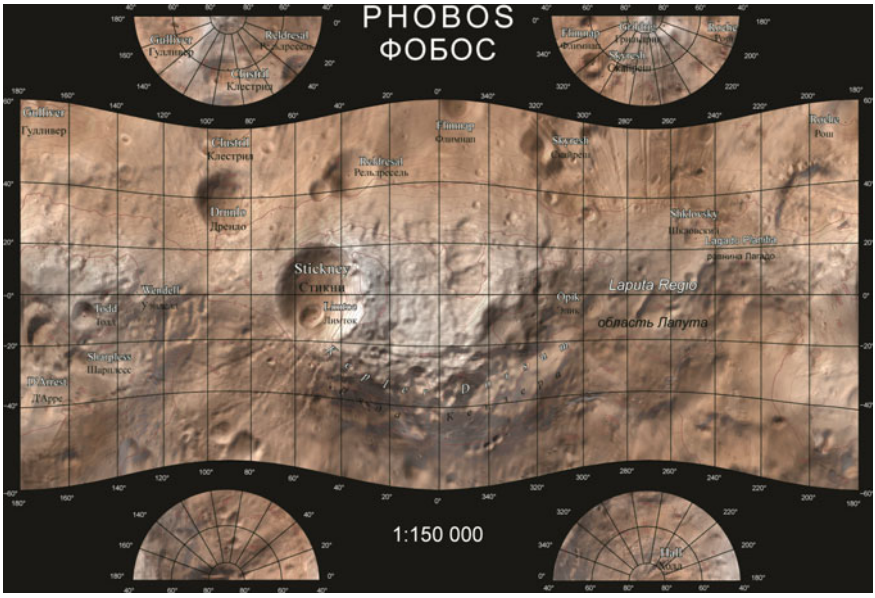


**Fig. 7.12** Topographic map from new Phobos atlas (MIIGAiK, 2015), based on new Mars Express SRC DTM (Karachevtseva et al. 2015): equatorial part: modified Bugaevsky (normal conformal cylindrical) projection for three-axial ellipsoid. Polar areas: Azimuthal equidistant along meridian projection for three-axial ellipsoid

distribution, density and area of geologic features and regions (Berthoud 2005). Clark et al. (2008) described the Constant Scale Natural Boundary (CSNB) map projection used for small, irregular body mapping. This projection allows relationships between noses, saddles, and poles to be observed without areal distortion.

## 7.6 Data Archive and Processing

Individual images sent back from space missions are stored in NASA's PDS in unprocessed (Experiment Data Record—EDR) raw data format. Some mission teams provide map-projected images, but many other images had to be processed by the individual researcher or mapper (Hare et al. 2014). The raw PDS images can be processed and map-projected to be cartography- and science-ready. Where available, images may be projected onto a DTM, and not a perfect sphere (Fig. 7.13).

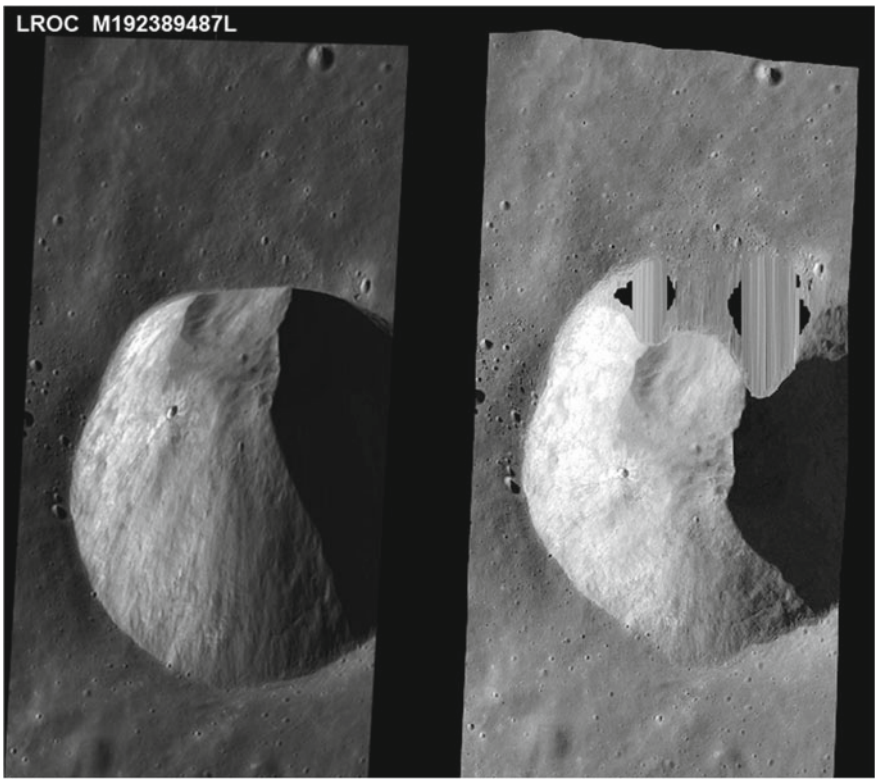


**Fig. 7.13** The view of a lunar crater in an unprocessed image (*left*) and a geometrically and radiometrically corrected image (*right*) that is projected onto a Lunar elevation model. Note the image fill of the crater wall that was not visible due to perspective viewing geometry

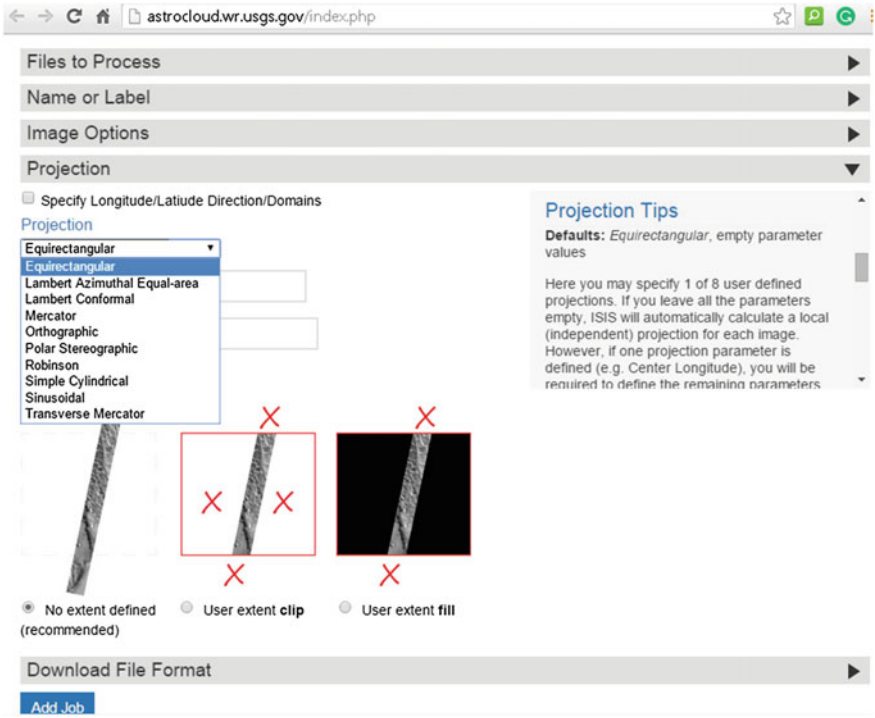


**Fig. 7.14** Job submission screen of POW, showing projection options and tips. (Captured 8/29/2015)

The most common image processing tool is ISIS (Integrated Software for Imagers and Spectrometers) developed by the Astrogeology Program of the United States Geological Survey for NASA. ISIS can be used for the radiometric and geometric/cartographic processing of the PDS raw images (Anderson et al. 2002). The projection modules of ISIS3 are used in the considerably more user-friendly Map Projection on the Web Service (POW) (Hare et al. 2013, 2014). POW supports ten different output projections (Fig. 7.14). Calibrated and projected images are ready to be imported to any GIS application where the display- or export-projection can be selected or defined by the user. Geospatial Data Abstraction Library (GDAL) can also be used for conversion from ISIS format to other, common image formats.

## 7.7 Conclusions

Controlled photomosaics and data-derived thematic planetary maps are a primary tool of mission planning and discovery for the professional planetary scientists (Christensen et al. 2009). Geological planetary maps interpret these data and serve

as a basis for subsequent studies. Features and characteristics of planetary surfaces are frequently studied in their fullness from pole to pole, and this task requires map displays that can be compared in local, regional and global scales and irrespectively of location, being either at the poles or at the equator.

**Acknowledgements** This work was compiled in the framework of the terms of reference of the International Cartographic Association Commission on Planetary Cartography. Some of the Mars related parts were supported by the COST TD1308 project.

## References

Akins SW, Hare TM, Sucharski RM, Shute J, Gaddis L, Gaither T, Richie J (2014) Map-a-planet 2 mosaic projection web service. In: 45th LPSC, abstract #2047

Alberz J, Gehrke S, Wählisch M, Lehmann H, Schumacher T, Neukum G, HRSC Co-Investigator Team (2004a) Digital cartography with HRSC on Mars express. In: International archives of photogrammetry and remote sensing (IAPRS), vol XXV, Istanbul, Part B4, pp 869–874

Alberz J, Jaumann R, Neukum G (2004b) Topographic image map of Mars 1:200.000 Albor Tholus region. Technical University of Berlin

Anderson JD (1975) Planetary geodesy. Rev Geophys Space Phys 13:274, 275, 292, 293

Anderson JA, Cook DA, Thompson KT (2002) Rapid geometric software development for scientific analysis and cartographic processing of planetary images. In: LPSC XXXIII, abstract #1853

Antoniadi EM (1930) La Planète Mars: étude basée sur les resultats obtenus avec la grande lunette de l'observatoire de Meudon et expose analytique de l'ensemble des travaux éxécutés sur cet astre depuis 1659. Libraire scientifique Hermann et cie, Paris

Archinal BA, Lee EM, Kirk RL, Duxbury TC, Sucharski RM, Cook DA, Barrett JM (2004) A new mars digital image model (MDIM 2.1) control network. In: XXth ISPRS Congress, Istanbul, Turkey, July 2004

Archinal BA, A'Hearn MF, Bowell E, Conrad A, Consolmagno G, Courtin R, Fukushima T, Hestroffer D, Hilton J, Krasinsky G, Neumann G, Oberst J, Seidelmann P, Stooke P, Tholen D, Thomas P, Williams I (2011) Report of the IAU working group on cartographic coordinates and rotational elements: 2009. Celest Mech Dyn Astr 109:101–135

Batson RM (1990) Cartography. In: Greeley R, Batson RM (eds) Planetary mapping. Cambridge University Press, Cambridge

Berthoud MG (2005) An equal-area map projection for irregular objects. Icarus 175(2):382–389

Bugaevsky LM (1987) On the problem of elaborating of isometric coordinates and equiangular cylinclric projection of the tri-axial ellipsoid. Izvestiya VUZov, ser Geod i Aerofot 4:79–90 (in Russian)

Bugaevsky LM (1999) The theory of map projections of the regular surfaces. M.: Zlatoust 144 (in Russian)

Bugaevsky LM, Krasnopevtseva BV, Shingareva KB (1992) Phobos map and phobos globe. Adv Space Res 12(9):17–21. doi:10.1016/0273-1177(92)90314-N

Burba GA (1996) Cartographic aspects of Venus global geologic mapping at 1:10,000,000 scale. Vernadskiy-Brown Micro 24 abstracts, Moscow, 11

Campbell DB, Dyce RB, Pettengill GH (1976) New radar image of Venus. Science 193:1123–1124

Carpenter RL (1966) Study of Venus by CW radar—1964 results. Astron J 71(2):142–152

Christensen PR, Engle E, Anwar S, Dickenshied S, Noss D, Gorelick N, Weiss-Malik M (2009) JMARS—a planetary GIS. American Geophysical Union, Fall Meeting 2009, abstract #IN22A-06. http://adsabs.harvard.edu/abs/2009AGUFMIN22A.06C

Clark PE, Clark CS, Stooke P (2008) Using boundary-based mapping projections for morphological classification of small bodies. In: LPSC XXXIX abstract #1371
Davies ME, Katayama FY (1984) The control network of Iapetus. Icarus 59:199–204
Davies ME, Rogers PG (1991) The preliminary geodetic control network of Venus. N-3437-JPL. A Rand Note
Davies ME, Abalakin VK, Brahic A, Bursa M, Chovitz BH, Lieske JH, Seidelmann PK, Sinclair AT, Tjuflin YS (1992) Report of the IAU/IAG/COSPAR working group on cartographic coordinates and rotational elements of the planets and satellites: 1991. Celest Mech Dyn Astron 53(4):377–397. doi:10.1007/BF00051818
Davies ME, Abalakin VK, Bursa M, Lieske JH, Morando B, Morrison D, Seidelman PK, Sinclair AT, Yallop B, Tjuflin YS (1995) Report of the IAU/IAG/COSPAR working group on cartographic coordinates and rotational elements of the planets and satellites: 1994. Celest Mech Dyn Astron 63(2):127–148. doi:10.1007/BF00693410
Davies ME, Colvin TR, Thomas P, Veverka J, Belton MJS, Oberst J, Zeitler W, Neukum G (1997) Control networks of the Galilean satellites: solutions for size and shape. In: LPSC XXVIII, abstract #1097
de Vaucouleurs G, Davies ME, Sturms FM Jr (1973) Mariner 9 areographic coordinate system. J Geophys Res 78:4395–4404
Di Palma V (2009) Zoom: google earth and global intimacy. In: Di Palma V, Periton D, Lathouri M (eds) Intimate metropolis: urban subjects in the Modern City. Routledge, pp 239–270
Duxbury TC, Kirk RL, Archinal BA, Neumann GA (2002) Mars geodesy/cartography working group recommendations on Mars cartographic constants and coordinate systems, ISPRS, vol 34, part 4. Geospatial Theory, Processing and Applications, Ottawa
Eliason E et al (2006) Software interface specification for HiRISE reduced data record products, mars reconnaissance orbiter, JPL Document Number D-32006, MRO-M-HIRISE-3-RDR-V1.0, NASA Planetary Data System
Flammarion C (1890) Mappemonde Géographique de la Planete Mars. In: Astronomie Populaire. Paris p 484
Flammarion C (1888 [1978]) Les fleuves de la planète Mars. Astronomie 457–462 (Reprinted in L'Astronomie 92, p 49)
Fleis ME (2004) Non-spherical coordinate systems transformations of the celestial bodies. Institute of Geography of the Russian Academy of Sciences, Russia (in Russian)
Gede M (2009) The projection aspects of digitising globes. ICC 2009, Chile, Santiago
Gehrke S, Wählisch M, Lehmann H, Schumacher T, Albertz J (2003) Cartography with HRSC on mars express—the new series "topographic image map mars 1:200,000". Publikationen der DGPF 12:451–458
Gehrke S, Wählisch M, Lehmann H, Albertz J, Roatsch T (2006) Generation of digital topographic maps of planetary bodies. In: International archives of photogrammetry and remote sensing (IAPRS), vol XXVI, Goa, Part B4
Google 2012 Map Types. https://developers.google.com/maps/documentation/javascript/maptypes#MapCoordinates
Greeley R, Batson RM (eds) (1990) Planetary mapping. Cambridge planetary science series, vol 6. Cambridge, New York, xiii+296 pp
Gwinner K, Scholten F, Preusker F, Elgne S, Roatsch T, Spiegel M, Schmidt R, Oberst J, Jaumann R, Heipke C (2010) Topography of Mars from global mapping by HRSC high-resolution digital terrain models and orthoimages: characteristics and performance. Earth Planet Sci Lett 294(3–4):506–519
Hare TM, Akins SW, Sucharski RM, Bailen MS, Anderson JA (2013) Map projection web service for PDS images. In: 44th LPSC, abstract #2068
Hare TM, Akins SW, Sucharski RM, Bailen MS, Shute J, Anderson JA, Gaddis LR (2014) POW: update for the PDS map projection web service. In: 45th LPSC, abstract #2474

Hargitai H, Bérczi S (2006) Multilingual maps of the terrestrial planets and their moons: the east and central european edition. European Planetary Science Congress Berlin, Germany, 18–22 Sept, pp 515

Hargitai H, Gede M (2009) Multilingual virtual globes of Venus and Mars. ICC 2009, Chile, Santiago

Hargitai H, Gede M, Zimbelman J, Kőszeghy C, Sirály D, Marinangeli L, Barata T, López I, Szakács A, Dębniak K, Feuillet T (2015) Multilingual narrative planetary maps for children. In: Sluter R, Madureira Cruz C, Bernadete C, de Menezes L, Márcio P (eds) Cartography—maps connecting the world. In: 27th international cartographic conference 2015. Springer, 17–30

Harris AW (1994) Tumbling asteroids. Icarus 107:209

Helled R, Anderson JD, Schubert G (2010) Uranus and Neptune: shape and rotation. Icarus 210:446–454

Hevelius (Johann Höwelcke) (1647) Selenographia sive lunae descriptio. Typis Hunefelianis, Gedani

Hirsch D (1994) Atlas of Venus I-2523 sheet 3 of 4. NASA-USGS

IAU (1971) Proceedings of the fourteenth general assembly (de Jagger C, Jappel A (ed) D. Reidel), Dordrecht

Inge JL, Batson RM (1992) Indexes of maps of the planets and satellites, NASA Technical Memorandum 4395

JPL (2009) Cartographic standards. In: Planetary data system standards reference. Version 3.8. JPL D—7669, part 2, Jet Propulsion Laboratory, California Institute of Technology, Pasadena, California

Karachevtseva IP, Kokhanov AA, Rodionova JR, Konopikhin AA, Zubarev AE, Nadezhdina IE, Mitrokhina LA, Patratiy VD, Oberst J (2015) Development of a new Phobos atlas based on Mars Express image data. Planetary and Space Science, Vol 108. pp. 24–30 doi: 10.1016/j.pss.2014.11.024

Kliore AJ, Cain DL, Fjeldbo G, Seidel BL, Sykes MJ, Rasool SI (1972) The atmosphere of Mars from mariner 9 radio occultation measurements. Icarus 17:484–516

Kneissl T, van Gasselt S, Neukum G (2011) Map-projection-independent crater size-frequency determination in GIS environments—new software tool for ArcGIS. Planet Space Sci 59: 1243–1254

Lazarev E, Rodionova J (2011) Venus mapping at small scale: source data processing and cartographic interpretation. In: Ruas A (ed) Proceedings of the 25th international cartographic conference. CO-160. ISBN: 978-1-907075-05-6

Lecacheux J, Combes M, Vapillon L (1973) The FI Scorpii occultation by Jupiter. I. The Jovian Diameter. Astron Astrophys 22:289

LGCWG: Lunar Geodesy and Cartography Working Group (2008) Recommendations for formatting large lunar datasets, May 18, draft

Lohse V, Heipke C, Kirk RL (2006) Derivation of planetary topography using multi-image shape-from-shading. Planet Space Sci 54(7):661–674

Márton M (ed) (2008) Virtual globes museum. http://vgm.elte.hu

Marov MY, Avduyevskiy VS, Borodin NF, Kerzhanovich VV, Lysov VP, Moshkin BY, Rozhdestvenskiy MK, Ryabov OL, Ekonoraov AP (1973) Preliminary results of measurements of the Venera 8 automatic spacecraft. NASA Technical Translation NASA TT F-14, 909

Marov MY, Krasnopevtseva BV, Shingareva KB (eds) (1992) Atlas of the terrestrial planets and their satellites. M. MIIGAiK, 208 p (in Russian)

Mayer T, Schröter JH (1791) Tob Mayeri Tabula Selenographica. In: Schröter JH: Selenotopographische Fragmente zur genauern Kenntniss der Mondfläche, ihrer erlittenen Veränderungen und Atmosphäre, sammt den dazu gehörigen Specialcharten und Zeichnungen. C.G. Fleckeisen, Lilienthal

McEwen AS, Eliason EM, Bergstrom JW, Bridges NT, Delamere WA, Grant JA, Gulick VC, Herkenhoff KE, Keszthelyi L, Kirk RL, Mellon MT, Squyres SW, Thomas N, Weitz CM (2007) MRO's high resolution imaging science experiment (HiRISE). J Geophys Res 112(E5). doi:10.1029/2005JE002605

MSSS: Malin Space Science Systems (2001) The martian prime meridian—longitude "zero" MGS MOC release No. MOC2-273, 31 Jan 2001. http://mars.jpl.nasa.gov/mgs/msss/camera/images/01_31_01_releases/airy0/

Muhleman DO (1961) Early results of the 1961 JPL Venus radar experiment. Astron J 66:292

NASA's PDS Geosciences Node at Department of Earth & Planetary Sciences in Washington University in St. Louis, Available online: http://geo.pds.nasa.gov/default.htm. Accessed 1 Sept 2015

Neumann GA, Rowlands DD, Lemoine FG, Smith DE, Zuber MT (2001) Crossover analysis of MOLA altimetric data. J Geophys Res 106:23723–23735

Neumann GA, Mazarico E, Smith DE, Zuber MT, Torrence MH, Barnouin OS, Solomon SC (2011) Laser altimetry of Mercury, Moon, and Mars. American Geophysical Union, Fall Meeting 2011, abstract #P41F-03

Newburn RL, Gulkis S (1973) A survey of the outer planets Jupiter, Saturn, Uranus, Neptune, Pluto, and their satellites. Space Sci Rev 14(2):179–271

Null GW (1976) Gravity field of Jupiter and its satellite from pioneer 10 and pioneer 11 tracking data. Astron J 81:1153–1161

Nyrtsov MV, Stooke PJ (2002) The mapping of irregularly-shaped bodies at planetary scale. In: Proceedings from international conference InterCarto 8. Helsinki–St. Petersburg, 28 May–1 June, pp 433–436

Nyrtsov MV, Fleis ME, Borisov MM (2012) Mapping of asteroid 433 Eros in cylindrical equidistant along the meridians and azimuthal projections triaxial ellipsoid. Izvestiya VUZov, ser. Geodesy Aerial Photogr 1:54–61 (in Russian)

Ostro SJ, Hudson RS, Rosema KD, Giorgini JD, Jurgens RF, Yeomans DK, Chodas PW, Winkler R, Rose R, Choate D, Cormier RA, Kelley D, Littlefair R, Benner LAM, Thomas ML, Slade MA (1999) Asteroid 4179 Toutatis: 1996 radar observations. Icarus 137:122–139

Proctor RA (1873) Half-hours with the telescope. G.P. Putnam's Sons, New York

Radebaugh J, Lorenz RD, Kirk RL, Lunine JI, Stofan ER, Lopes RMC, Wall SD, Cassini RADAR Team (2007) Mountains on Titan observed by Cassini Radar. Icarus 192(1):77–91

Roatsch T, Wälisch M, Giese B, Hoffmeister A, Matz K-D, Scholten F, Kuhn A, Wagner R, Neukum G, Helfenstein P, Porco C (2008) High-resolution Enceladus atlas derived from Cassini-ISS images. Planet Space Sci 56:109–116

Rosiek MR, Howington-Kraus E, Hare TM, Redding BL (2003) Mars transverse mercator (MTM) map series updated with plan-etocentric grid, lunar and planetary science, XXXIV, Lunar and Planetary Institute, Houston, unpaginated CD-ROM, abstract 1371

Rosiek MR, Kirk RL, Archinal BA, Howington-Kraus E, Hare T, Galuszka D, Redding B (2005) Utility of viking orbiter images and products for Mars mapping. Photogram Eng Remote Sens 71(10):1187–1195

Seidelmann PK, Abalakin VK, Bursa M, Davies ME, de Bergh C, Lieske JH, Oberst J, Simon JL, Standish EM, Stooke P, Thomas PC (2002) Report of the IAU/IAG working group on cartographic coordinates and rotational elements of the planets and satellites: 2000. Celest Mech Dyn Astron 82(1):83–111. doi:10.1023/A:1013939327465

Seidelmann PK, Archinal BA, A'Hearn MF, Conrad A, Consolmagno GJ, Hestroffer D, Hilton JL, Krasinsky GA, Neumann G, Oberst J, Stooke P, Tedesco E, Tholen DJ, Thomas PC, Williams IP (2007) Report of the IAU/IAG working group on cartographic coordinates and rotational elements: 2006, Celestial Mechanics and Dynamical Astronomy, vol 98, pp 155–180 [WGCCRE #10]

Shingareva KB, Zimbelman J, Buchroithner MF, Hargitai HI (2005) The realization of ICA commission projects on planetary cartography, Cartographica, vol 40, no. 4/Winter 2005. doi:10.3138/3660-4078-55X1-3808

Simonelli DP, Thomas PC, Carcich BT, Veverka J (1993) The generation and use of numerical shape models for irregular solar system objects. Icarus 103:49–61

Smith DE, Zuber MT, Solomon SC, Phillips RJ, Head JW, Garvin JB, Banerdt WB, Muhleman DO, Pettengill GH, Neumann GA, Lemoine FG, Abshire JB, Aharonson O,

Brown CD, Hauck SA, Ivanov AB, McGovern PJ, Zwally HJ, Duxbury TC (1999) The global topography of Mars and implications for surface evolution. Science 284:1495–1503

Smith DE, Zuber MT, Neumann GA, Lemoine FG, Mazarico E, Torrence MH, McGarry JF, Rowlands DD, Head JW, Duxbury TH, Aharonson O, Lucey PG, Robinson MS, Barnouin OS, Cavanaugh JF, Sun X, Liiva P, D-d Mao, Smith JC, Bartels AE (2010) Initial observations from the lunar orbiter laser altimeter (LOLA). Geophys Res Lett 37:L18204. doi:10.1029/2010GL043751

Stooke P (1992) Cartography of asteroids and comet nuclei from low resolution data. Asteroids, Comets, Meteors 1991. LPI, Houston, pp 583–586

Tanaka KL, Skinner JA Jr, Dohm JM, Irwin RP III, Kolb EJ, Fortezzo CM, Platz T, Michael GG, Hare TM (2014) Geologic map of Mars: U.S. Geological Survey Scientific Investigations Map 3292, scale 1:20,000,000, pamphlet 43 p. http://dx.doi.org/10.3133/sim3292

Thomas PC (1989) The shapes of small satellites. Icarus 77:248–274

Thomas PC, Joseph J, Carcich B, Veverka J, Clark BE, Bell JF, Byrd AW, Chomko R, Robinson M, Murchie S, Prockter L, Cheng A, Izenberg N, Malin M, Chapman C, McFadden LA, Kirk R, Gaffey M, Lucey PG (2002) Eros: shape, topography, and slope processes. Icarus 155:18–37

USGS (2003) Topographic map of Mars. Geologic Investigations Series i–2782

USGS (n.d.) Arcadia, MC-3. http://planetarynames.wr.usgs.gov/images/mc3_mola.pdf

Veverka J (1985) Planetary geology in the 1980s. NASA Office of Space Science and Applications, Washington DC

Wagner K (1962) Kartographische Netzentwürfe. Bibliografisches Institut Mannheim. pp 155–156

Whitaker EA (2003) Mapping and naming the moon: a history of lunar cartography and nomenclature. Cambridge University Press, pp 264

Wilhelms DE (1987) The geologic history of the Moon. USGS Professional Paper 1348. pp 11

Wilhelms DE (1990) Geologic mapping. In: Greeley R, Batson RM (eds) Planetary mapping. Cambridge University Press, New York, pp 208–260

Willner K, Oberst J, Hussmann H, Giese B, Hoffmann H, Matz KD, Roatsch T, Duxbury T (2010) Phobos control point network, rotation, and shape. Earth Planet Sci Lett 294:541–546

Wilson LJ (1912) A Mercator's projection of Mars. Popular Astron 20:65–65

Wu SSC (1991) Topographic maps of the polar, western, and eastern regions of Mars, Scale 1:15,000,000, U.S. Geological Survey Map I-2160

Zangari A (2015) A meta-analysis of coordinate systems and bibliography of their use on Pluto from Charon's discovery to the present day. Icarus 246:93–145

Zuber MT, Smith DE (1998) The relationship of MOLA northern hemisphere topography to the 6.1 mbar atmospheric pressure surface of Mars. In: 29th LPSC, 16–20 Mar 1998, Houston, TX, abstract #1724